

Renewable energy liberation by nonthermal intermolecular bond dissociation in water and ethanol

N. Graneau,^{1,a)} S. Verdoold,² G. Oudakker,³ C. U. Yurteri,² and J. C. M. Marijnissen^{2,3}

¹*AWE, Aldermaston, RG7 4PR United Kingdom*

²*Applied Sciences, TU Delft, 2628BL Delft, The Netherlands*

³*WETSUS, Centre of Excellence for Sustainable Water Technology, 8934CJ Leeuwarden, The Netherlands*

(Received 9 January 2010; accepted 13 December 2010; published online 14 February 2011)

Prior indication that renewable energy can be extracted from hydrogen bonds in water has led to several investigations of the energy balance when bulk liquid is converted into micron scale droplets by directional (nonthermal) forces. The demonstration of this effect has previously involved pulsed high current arcs in water which produce large electrodynamic forces. Here, we show that renewable energy is also liberated during the creation of droplets by electrostatic forces in electrohydrodynamic atomization (electrospray) experiments. Using both ethanol and water, the energy outputs, primarily the droplet kinetic energy, were always greater than the energy inputs, implying that stored energy was liberated from the liquid. The energetics of generic chemical bonding are investigated to demonstrate that although this discovery was not publicly anticipated, it is consistent with conventional theory. This experimental breakthrough should have a major impact on the quest for renewable energy sources, capable of powering electricity generators. © 2011 American Institute of Physics. [doi:10.1063/1.3544497]

I. INTRODUCTION

Several papers^{1,2} have reported that under certain conditions, the rapid dissociation of liquid water into micron scale droplets in pulsed high current arcs in water is accompanied by the release of kinetic energy which had been previously stored in the liquid bonding network. The explosion results in droplets which have been reported to exhibit more kinetic energy than the electrical energy supplied, implying the liberation of energy which could only have been initially stored in the liquid. The storage and release of potential energy in intermolecular bonds, in this case hydrogen bonds in water, is a relatively unexplored renewable energy source which may play a crucial role in resolving the impending global energy and climate crises.

Unfortunately, the transient nature of water arc explosions has prevented the accurate correlation of droplet mass and velocity in the resulting expansion and therefore, only indirect energy measurements have been performed. In an effort to more directly demonstrate the liberation of stored intermolecular bond energy, a lower density, stationary (identical conditions preserved for a sustained time period) experiment was devised, and the results are presented here. In this experiment, electrostatic forces cause break up of a thin jet of liquid into an aerosol of droplets in a process known as electrohydrodynamic atomization (EHDA) or electro-spraying.³

An energy balance of the EHDA mechanism has been performed in which the energy inputs which are required to form the aerosol spray were measured as well as some of the energy outputs, specifically the total kinetic energy of the spray as well as the amount of energy which has been stored as increased surface tension energy in the newly formed

droplets. This demonstrated that under certain conditions the energy output was greater than the energy input and therefore, that stored potential energy is liberated during the EHDA process.

In order to perform this technique, a fine stream of liquid is pumped downward from a vertically mounted capillary nozzle electrode toward a lower flat electrode at a high negative potential. In general, the emerging liquid becomes charged by the resulting electric field. Under the appropriate conditions of flow rate and electric field intensity, the liquid meniscus is changed into a stationary or pulsating cone with a jet at its apex which breaks up into charged droplets. These droplets then disperse toward the planar electrode in an expanding cone of radial symmetry.

The high surface tension of water makes it a nonideal electro-spraying liquid, nevertheless, measurements have revealed that stored energy was liberated during the aerosol formation. To demonstrate that this effect occurs to a greater or lesser extent in other liquids, all of which contain an intermolecular bonding network, the energy gain was also successfully demonstrated with ethanol, a liquid of lower surface tension, with which it is easier to create a stable stationary spray. This experiment has provided the most convincing demonstration to date that liquids contain a source of stored energy which can be liberated during the nonthermal conversion to droplets.

The storage of renewable energy in intermolecular bonds is shown to be consistent with conventional chemical bonding theory. However, unlike the latent heat, the quantity of stored energy for different substances is never tabulated as it is rarely if ever measured. This has occurred because the conventional method of quantitative injection and extraction of energy from chemical bonds is via the relatively slow process of thermal energy transfer by multiple collisions. The

^{a)}Electronic mail: neal.graneau@awe.co.uk.

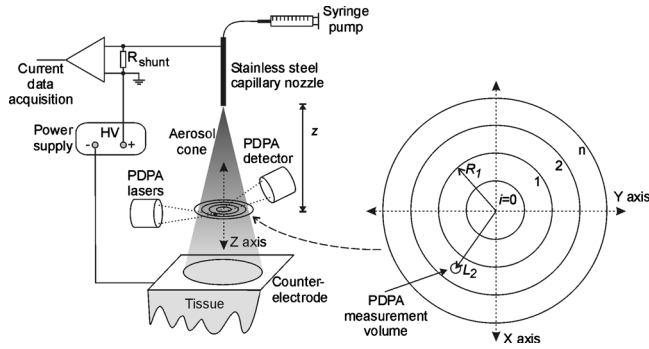


FIG. 1. Schematic depiction of experimental set-up including a depiction of the sampling zones used to estimate properties of the total liquid flow through a plane z mm below the nozzle.

experiments described here demonstrate that the more rapid intermolecular bond dissociation by directed electrostatic forces can efficiently convert the stored energy into directed kinetic energy. Such results point the way forward toward a new arena of research and development into the optimization of technologies which can harness this novel renewable energy resource.

II. EXPERIMENTAL CONFIGURATION AND METHODS

The EHDA experimental set-up is illustrated in Fig. 1. The liquid was pumped through a 1.5 mm inner diameter (id) stainless steel capillary tube by a syringe pump with a controllable flow rate of $\pm 1\%$ accuracy. A high voltage (HV) power supply imposed negative voltage on a 20 mm wide flat electrode, a fixed distance below the capillary nozzle. The flat electrode collected all of the positively charged aerosol spray, thus forming a complete electrical circuit. In order to avoid liquid from building up on the flat electrode, a thin sheet of tissue was draped over it to drain the excess. Current was measured by a differential amplifier monitoring the voltage across a resistor inserted in the circuit between the nozzle and the grounded positive side of the HV supply. The primary diagnostic tool was a TSI-Aerometrics phase Doppler particle analyzer (PDDPA), which allowed the gathering of a statistical survey of the correlated droplet size and vertical and horizontal velocity components passing through a small sampling volume. This measurement region could be positioned at many places in the aerosol cone, allowing a statistical determination of the total kinetic and surface tension energy passing through a given plane per second.

A. Energy outputs

The EHDA process produces a steady flow system and it is therefore, logical to quantify the fundamental energy components in units of power (watt). Once the stationary spray system has been created, its power output can be quantified by four components; P_{KIN} , (kinetic energy), P_{SURF} , (surface tension), P_{DRAG} , (air friction heating), and P_{ION} (ionization). These are defined below:

1. P_{KIN}

A two component laser-Doppler velocimeter (LDV)/PDDPA was used to measure the size and velocity of the liquid

droplets in the aerosol spray. In general, a single laser beam is split into two equal intensity beams, which cross each other at a point in the droplet flow field and define the measurement volume. In a two component LDV, an additional pair of laser beams with different wavelengths from the first pair are crossed at the same point, allowing measurement of the droplet velocity in two orthogonal directions. When a single droplet is detected in this region, its diameter and both vertical and horizontal velocity components are deduced and recorded on a dedicated computer.

A method was developed to assess the rate of total kinetic energy passing through a horizontal plane at a fixed distance, z , below the nozzle. The cross-sectional area of this plane was divided into a circular central section and n surrounding annular sections as shown in Fig. 1. n is required to be large enough to ensure that all of the spray droplets pass through one of the regions. The radius of the central section and the thickness of the annuli are designed to be narrow enough so that it can be assumed that the spray properties (droplet size, kinetic energy, and mass flow rate) are uniform throughout the region. In order to estimate the total kinetic energy passing through a predetermined plane per second, P_{KIN} , the PDDPA must sample the spray parameters for at least one time interval in each region in conjunction with knowledge of the total mass flow rate leaving the nozzle.

The Cartesian axes used to define the location of the measurement region are also shown in Fig. 1. The Z-axis is vertical and represents the direction in which the LDV system measures the vertical droplet velocity and the origin is the center of the central circular region for the plane under measurement. The X-axis is defined as the direction in which the LDV system measures the horizontal velocity. Therefore, velocity components parallel to the Y-axis are not detected. Hence the recorded total velocity is always a conservative (low) estimate. The origin is discovered experimentally by looking for symmetry in the droplet horizontal velocity.

For a given distance below the nozzle, z , M_i measurement intervals are captured in one or several locations in region i over one or more time periods of duration, $t_{i,j}$ and during these intervals $N_{i,j}$ droplets are detected and measured. Therefore, the detected liquid volume flow rate, $\Phi_{i,z}$, through the sampling cross-sectional area in region i at height z , can be represented as

$$\Phi_{i,z} = \frac{1}{M_i} \sum_{j=1}^{M_i} \left(\frac{1}{t_{i,j}} \frac{\pi}{6} \sum_{\ell=1}^{N_{i,j}} d_{j,\ell}^3 \right). \quad (1)$$

Since each detected droplet with diameter $d_{j,\ell}$ has both a measured vertical and horizontal velocity component, $v_{v,j,\ell}$ and $v_{h,j,\ell}$, respectively, then the detected kinetic energy flowing through the PDDPA measurement volume in region i at height, z , per unit time is

$$P_{KIN, meas, i, z} = \frac{1}{M_i} \sum_{j=1}^{M_i} \left(\frac{1}{t_{i,j}} \frac{1}{2} \rho \frac{\pi}{6} \sum_{\ell=1}^{N_{i,j}} d_{j,\ell}^3 (v_{v,j,\ell}^2 + v_{h,j,\ell}^2) \right), \quad (2)$$

where ρ is the density of the liquid under investigation. Neither the precise horizontal cross-sectional area of the PDDPA measurement volume nor the droplet detection efficiency are known accurately. However, both of these parameters are

considered to be constant throughout the experiment. Therefore, in order to estimate the total kinetic energy that passes through the entire measurement plane per second, $P_{KIN,z}$, at a height z below the nozzle, a constant, k_z , can be defined as

$$k_z = \frac{f}{\sum_{i=0}^n \left(\frac{A_i}{A_{total}} \Phi_{i,z} \right)}, \quad (3)$$

where f is the measured flow rate produced by the syringe pump, which is assumed to represent the total volume of droplets per second passing through the regions 0– n at all heights, z , in which the area of the i 'th region is A_i and the area of all the regions together is A_{total} . In this case

$$P_{KIN,z} = k_z \sum_{i=0}^n \left(\frac{A_i}{A_{total}} P_{KIN,meas,i,z} \right). \quad (4)$$

Statistical averages for the droplet diameter and velocity components have been deduced for each PDPA measurement period (i, j). It is more accurate however, to allow the dedicated PDPA computer analysis software to calculate the required summations over the index, ℓ , in Eqs. (1) and (2). Therefore, as a result of subdividing the measurement plane into n radially symmetric regions as shown in Fig. 1 and ensuring that at least one PDPA measurement is taken in each area, Eq. (4) allows an estimate of the total kinetic energy power flow at a given height, z , below the nozzle.

2. P_{SURF}

In the conversion from bulk liquid to droplets, the liquid surface area in the system is being increased dramatically. The PDPA data was employed to discover the rate at which potential energy was being stored as increased liquid surface area. If σ (N/m) represents the surface tension constant of the liquid under investigation, then the surface energy of a spherical droplet of diameter, d , is given by $(\pi d^2 \sigma)$. Using the terminology from the previous section, the detected surface tension energy passing through the PDPA measurement volume per unit time in sector, i , and height, z , is

$$P_{SURF,meas,i,z} = \frac{1}{M_i} \sum_{j=1}^{M_i} \left(\frac{1}{t_{i,j}} \pi \sigma \sum_{\ell=1}^{N_{i,j}} d_{j,\ell}^2 \right). \quad (5)$$

The summation over the index, ℓ , was again performed by the dedicated PDPA analysis software. Using the same constant of proportionality, k_z , defined in Eq. (3), the total rate of surface energy passing through a measurement plane at a fixed height, z , below the nozzle is

$$P_{SURF,z} = k_z \sum_{i=0}^n \left(\frac{A_i}{A_{total}} P_{SURF,meas,i,z} \right). \quad (6)$$

3. P_{DRAG}

The spray passes through the air, which generates a consequent amount of heat and thermal power as a result of friction drag. The data reveals that the kinetic energy of the droplets does not change significantly despite the acceleration due to the electric field, thus implying that air drag is

significant although difficult to measure without precise calorimetry which was not performed in this experiment.

4. P_{ION}

Under certain conditions, the electric field near the nozzle is sufficient to cause ionization of the surrounding air and consequent coronal discharge. This represents unmeasured current and is hence a power output which is difficult to quantify directly. It is shown later that all experiments presented here were performed under the ionization threshold potential and this term is therefore, negligible.

B. Energy inputs

The aerosol spray receives power by four separate mechanisms, P_{ELEC} , (electric power), P_{PUMP} , (pump power), P_{GRAV} , (gravity), and $P_{SURF,I}$, (initial surface tension). These are defined below:

1. P_{ELEC}

The largest energy input to the EHDA process is electrical power by several orders of magnitude. The electric potential between the nozzle and collector is created by the dc HV power supply. A suitable liquid flow rate is then set by the syringe pump which produces a steady flow of droplets with a narrow size distribution. These two parameters determine the current in the circuit which is measured by monitoring the voltage across a 99.7 k Ω . shunt resistance with a INA110KP fast-settling, field effect transistor -input, very high accuracy instrumentation amplifier with a bandwidth of at least 50 kHz and only dropping 15% at 100 kHz. As shown in Fig. 1, the shunt resistor was inserted between the HV power supply and the nozzle electrode to ensure that all of the power supply current was detected. The amplifier output was sampled at 200 kHz by a computer driven data acquisition interface. Dedicated software performed a numerical average of the current over several measurement periods of 12.5 s each, revealing a fairly steady average current level, I_{av} , over the course of the several tens of minutes required to sample all of the data for a particular height, z . This average current value multiplied by the HV output of the power supply, V , yields a measure of the electrical power flowing in the circuit as

$$P_{ELEC} = I_{av} V. \quad (7)$$

2. P_{PUMP}

The liquid enters the EHDA system with a mass flow rate of (ρf) and a velocity of (f/A_{cap}) where f is the liquid volume flow rate, ρ is the liquid density and A_{cap} and d_{cap} are, respectively, the cross sectional area and inner diameter of the capillary tube nozzle. The kinetic energy delivered to the EHDA system per second is, therefore

$$P_{PUMP} = \frac{1}{2} \rho f \left(\frac{f}{A_{cap}} \right)^2 = \frac{8 \rho f^3}{\pi^2 d_{cap}^4}. \quad (8)$$

3. P_{GRAV}

With the pump not running, liquid is not emitted from the nozzle since the attractive interaction with the metal tube prevents gravitational acceleration of the water. Therefore, during the EHDA spraying, the liquid only gains kinetic energy from gravity after it has left the nozzle. If g is the acceleration due to gravity then at a particular measurement height below the capillary tube, z , the kinetic energy passing through the plane per second due to gravitational force is

$$P_{GRAV,z} = \rho f g z. \quad (9)$$

4. $P_{SURF,I}$

The bulk liquid already stores some surface energy prior to breaking up into droplets. To determine the surface area of the liquid meniscus⁴ at the nozzle is, however, very difficult. It was therefore, decided to estimate it by calculating the surface area of a hemisphere with a diameter equal to the inner diameter of the capillary ($(1/2)\pi d_{cap}^2$). This surface is constantly being broken up and re-created at a rate consistent with the total liquid flow rate, f . Given that the volume of the hemisphere is $((1/12)\pi d_{cap}^3)$ then the rate of liquid surface creation is $(6f/d_{cap})$. Therefore, the rate of liquid surface tension energy entering the EHDA system just prior to the breaking up into droplets is

$$P_{SURF,I} = \frac{6f\sigma}{d_{cap}}. \quad (10)$$

C. Efficiency measurement

The inability to measure the air drag and ionization losses means that only a minimum or conservative estimate of the efficiency of the EHDA process, $\eta_{min,z}$, can be determined, defined by

$$\eta_{min,z} = \frac{P_{KIN,z} + P_{SURF,z}}{P_{ELEC} + P_{PUMP} + P_{GRAV,z} + P_{SURF,I}}. \quad (11)$$

Equation (11) can be assessed independently at each measurement height, z .

III. EXPERIMENTAL DETAILS

A. Measurements with ethanol

An EHDA produced ethanol electrospray was created with a flow rate, f , (4 mL/h) through the capillary and the counter electrode was located 15 mm below the nozzle with a potential difference of 6.3 kV between them. The spray mode used for the measurements was selected to minimize the voltage and prevent ionization and yet create a steady spray indicated by a primarily dc current with a steady high frequency ripple. The spray was analyzed at three distances, z , below the nozzle, at which the PDPA surveyed the properties of the aerosol to gain a value of the kinetic and surface tension energy power flowing through the horizontal plane according to the methodology outlined in Eqs. (1)–(6).

The recorded data is displayed in Table I, in which the regions of each measurement plane were defined as zone ($i=0$) being circular and the other regions ($i \geq 1$) being annu-

lar. These regions with outer radii, R_i , were designed to be narrow enough to justify the assumption that the spray properties are uniform throughout each zone while keeping the PDPA measurement location, L_i , (distance from Z-axis) as near to the center of the annular width as possible. In several cases, measurements were taken at the same radial distance from the axis but in differing places in the annular region, which on all occasions supported the assumption of radial symmetry. A demonstration of this symmetry is presented in the next section describing a water electrospray. $d_{i,z}$ is the average droplet diameter in region i at height, z . At all heights, measurements were performed at increasing distances away from the axis until the flow rate fell below 1 detected droplet per second which is less than 0.1% of the maximum rate.

The detected volume flow rate, $\Phi_{i,z}$, defined by Eq. (1) is listed for each region in Table I. These values are required to calculate a constant of proportionality for each height, k_z , using Eq. (3), assuming that the liquid volume flow rate through the measurement plane was the same as that leaving the nozzle, f .

By performing one or more sampling periods in each region, a kinetic power measurement for each zone, $P_{KIN,meas,i,z}$, could be determined, defined by Eq. (2) and shown in Table I. Each of these quantities was then multiplied by $[k_z(A_i/A_{total})]$ and summed, yielding a value of the total liquid kinetic energy flowing through the plane per second, $P_{KIN,z}$, according to Eq. (4) and displayed in Table II.

The same PDPA measurements were analyzed according to Eq. (5), revealing the detected surface tension energy passing through the PDPA volume per second, $P_{SURF,meas,i,z}$, and listed in Table I. These figures can be multiplied by $[k_z(A_i/A_{total})]$ and summed, providing a value for the total surface tension energy passing through the plane per second, $P_{SURF,z}$ according to Eq. (6) and also summarized in Table II.

The electrical power measurement P_{ELEC} in Table II is the result of averaging the power levels calculated over 12.5 s sampling periods with Eq. (7) during each PDPA measurement interval at a particular height. Inspection of a current trace in detail revealed a stationary high frequency oscillation (~ 55 kHz) around a dc signal as shown in Fig. 2. A power spectrum of the signal revealed that 97% of the power is present at 0 Hz (dc), indicating that the system can be considered stationary, justifying the use of the average current and voltage to estimate the constant electrical power flow through the circuit. The current oscillation has been attributed to pulsation of the geometry of the emitting meniscus,⁵ which acts as a varying capacitance. The total voltage produced by the high impedance HV power supply is therefore, negligibly affected by the measured current oscillations and can therefore, be considered to be a steady dc voltage for the purpose of calculating the electric power in the circuit in Eq. (7). It has been shown in⁶ that the current oscillation frequency is a complex function of the voltage, flow rate, nozzle geometry and the electrical conductivity of the liquid.

P_{PUMP} , $P_{GRAV,z}$, and $P_{SURF,I}$ can be determined from Eqs. (8)–(10) with knowledge of f , (4 mL/h) the liquid flow

TABLE I. PDPA data from experiments with ethanol and water.

Liquid	z (mm)	i	L_i (mm)	R_i (mm)	$d_{i,z}$ (μm)	$\Phi_{i,z}$ (m^3/s)	$P_{KIN,meas,i,z}$ (μW)	$P_{SURF,meas,i,z}$ (μW)
Ethanol	6.5	0	0.25	0.50	15.3	7.29×10^{-13}	5.93×10^{-2}	4.93×10^{-3}
Ethanol	6.5	1	0.75	0.84	21.4	7.92×10^{-11}	7.89×10^0	4.80×10^{-1}
Ethanol	6.5	2	1.00	1.16	20.6	2.07×10^{-11}	2.03×10^0	1.29×10^{-1}
Ethanol	6.5	3	1.25	1.34	17.0	2.17×10^{-12}	1.72×10^{-1}	1.60×10^{-2}
Ethanol	6.5	4	1.50	1.66	11.0	2.60×10^{-13}	1.02×10^{-2}	2.66×10^{-3}
Ethanol	8.5	0	0.25	0.50	17.7	1.08×10^{-12}	6.98×10^{-2}	7.59×10^{-3}
Ethanol	8.5	1	0.75	1.00	18.9	2.60×10^{-11}	2.35×10^0	1.56×10^{-1}
Ethanol	8.5	2	1.25	1.50	22.0	2.36×10^{-11}	2.02×10^0	1.38×10^{-1}
Ethanol	8.5	3	1.75	2.00	18.9	9.83×10^{-13}	6.78×10^{-2}	6.60×10^{-3}
Ethanol	8.5	4	2.25	2.50	12.4	2.32×10^{-13}	6.68×10^{-3}	2.31×10^{-3}
Ethanol	10.5	0	0.25	0.51	18.1	1.13×10^{-12}	9.17×10^{-2}	8.16×10^{-3}
Ethanol	10.5	1	0.75	1.16	18.0	3.49×10^{-11}	3.37×10^0	2.14×10^{-3}
Ethanol	10.5	2	1.75	1.93	8.2	1.03×10^{-13}	1.47×10^{-3}	8.91×10^{-5}
Ethanol	10.5	3	2.25	2.57	6.1	1.02×10^{-14}	4.05×10^{-3}	1.30×10^{-3}
Water	3	0	0.00	0.50	7.1	1.23×10^{-13}	3.17×10^{-2}	6.48×10^{-3}
Water	3	1	1.00	1.50	7.0	1.69×10^{-14}	4.37×10^{-3}	8.70×10^{-4}
Water	3	2	2.00	2.50	7.9	1.81×10^{-15}	3.61×10^{-4}	8.61×10^{-5}
Water	5	0	0.00	0.50	10.0	5.38×10^{-13}	9.03×10^{-2}	1.16×10^{-2}
Water	5	1	1.00	1.55	7.9	9.34×10^{-14}	1.55×10^{-2}	3.76×10^{-3}
Water	5	2	2.00	2.47	7.4	8.98×10^{-14}	1.13×10^{-2}	4.47×10^{-3}
Water	5	3	3.00	3.39	7.5	2.44×10^{-14}	2.72×10^{-3}	1.23×10^{-3}
Water	5	4	3.50	3.61	8.4	6.75×10^{-16}	5.86×10^{-5}	3.23×10^{-5}
Water	5	5	4.00	4.53	8.9	1.20×10^{-14}	1.20×10^{-3}	5.09×10^{-4}
Water	5	6	5.00	5.47	9.9	3.94×10^{-15}	3.64×10^{-4}	1.52×10^{-4}
Water	8	0	0.00	0.50	8.3	1.54×10^{-13}	1.24×10^{-2}	5.24×10^{-3}
Water	8	1	1.00	1.47	9.7	1.27×10^{-13}	1.09×10^{-2}	3.69×10^{-3}
Water	8	2	2.00	2.53	7.5	8.27×10^{-14}	5.97×10^{-3}	3.94×10^{-3}
Water	8	3	3.00	3.47	7.7	6.54×10^{-14}	4.56×10^{-3}	3.07×10^{-3}
Water	8	4	4.00	4.53	7.8	4.20×10^{-14}	2.85×10^{-3}	1.98×10^{-3}
Water	8	5	5.00	5.47	8.3	2.68×10^{-14}	1.74×10^{-3}	1.24×10^{-3}
Water	8	6	6.00	6.53	8.0	2.61×10^{-14}	1.54×10^{-3}	1.21×10^{-3}
Water	8	7	7.00	7.47	8.4	1.54×10^{-14}	8.53×10^{-4}	6.95×10^{-4}
Water	8	8	8.00	8.53	9.4	5.84×10^{-15}	3.09×10^{-4}	2.48×10^{-4}
Water	13	0	0.00	0.50	8.8	6.52×10^{-14}	4.27×10^{-3}	2.11×10^{-3}
Water	13	1	1.00	1.60	8.3	4.98×10^{-14}	3.22×10^{-3}	1.92×10^{-3}
Water	13	2	2.00	2.40	8.2	4.71×10^{-14}	2.93×10^{-3}	1.93×10^{-3}
Water	13	3	3.00	4.00	8.3	6.88×10^{-14}	4.27×10^{-3}	2.98×10^{-3}
Water	13	4	5.00	6.00	8.3	2.29×10^{-14}	1.47×10^{-3}	1.03×10^{-3}
Water	13	5	7.00	8.00	11.9	2.57×10^{-15}	2.20×10^{-4}	8.58×10^{-5}
Water	19.5	0	0.00	1.00	19.0	8.89×10^{-14}	6.05×10^{-3}	9.39×10^{-4}
Water	19.5	1	2.00	3.00	8.1	2.83×10^{-14}	2.23×10^{-3}	1.27×10^{-3}
Water	19.5	2	4.00	5.00	8.1	2.29×10^{-14}	1.62×10^{-3}	1.07×10^{-3}
Water	19.5	3	6.00	7.00	8.1	1.47×10^{-14}	1.06×10^{-3}	7.11×10^{-4}
Water	19.5	4	8.00	8.30	7.9	6.75×10^{-15}	5.63×10^{-4}	3.37×10^{-4}
Water	19.5	5	9.00	10.00	10.2	1.52×10^{-15}	1.71×10^{-4}	6.12×10^{-5}

rate through the nozzle, d_{cap} , (1.5 mm) the id of the capillary tube and ρ and σ , the density and surface tension of ethanol, respectively (0.789 g/cm³ and 0.022 N/m).

Using Eq. (11), a minimum estimate for the efficiency of the EHDA process for the three heights, z , was determined as shown in Table II and Fig. 3(a), which ranged between 3.05–3.41 \pm 16%. It can be seen that the kinetic energy of the ethanol was roughly the same at all three heights, despite being continuously pulled through an electric field. This indicates that the air friction losses must be significant and the actual EHDA efficiency may have been higher than 300%. This result directly demonstrates observed energy gain,

which must be the result of energy liberated from intermolecular bonds during the EHDA conversion from bulk to droplets.

B. Measurements with water

A set of experiments, similar to those just described, were performed with water. Despite using a proprietary nozzle specifically designed for producing an EHDA water aerosol, production of a monodisperse water electrospray was not achieved. This is thought to be due to the significantly higher surface tension of water (0.073 N/m) compared

TABLE II. Analyzed PDPA data including a minimum EHDA efficiency estimate for ethanol and water.

Liquid	z (mm)	d_z (μm)	P_{ELEC} (μW)	$P_{SURF,i}$ (μW)	P_{PUMP} (μW)	$P_{GRAV,z}$ (μW)	$P_{KIN,z}$ (μW)	$P_{SURF,z}$ (μW)	$\eta_{min,z}$	$\Delta\eta/\eta$
Ethanol	6.5	18.3	33.9	0.098	1.73×10^{-7}	0.056	109	6.82	3.41	0.14
Ethanol	8.5	19.1	33.4	0.098	1.73×10^{-7}	0.073	95.8	6.65	3.05	0.16
Ethanol	10.5	17.5	33.9	0.098	1.73×10^{-7}	0.090	106	6.73	3.30	0.12
Water	3.0	6.87	139	1.25	1.15×10^{-5}	0.122	1051	214	9.04	0.20
Water	5.0	7.37	163	1.25	1.15×10^{-5}	0.203	562	177	4.48	0.10
Water	8.0	7.51	146	1.25	1.15×10^{-5}	0.327	282	184	3.15	0.07
Water	13.0	7.83	148	1.25	1.15×10^{-5}	0.529	267	177	2.97	0.13
Water	19.5	8.13	166	1.25	1.15×10^{-5}	0.795	314	184	2.96	0.12

to ethanol (0.022 N/m). Consequently a higher voltage was required which caused coronal discharge into the air and an erratic current signal, thus the EHDA efficiency could not be discerned. Earlier research⁷ had indicated that CO₂, despite having a lower breakdown strength than air has a higher electron affinity and can thus suppress the coronal discharge for moderate water flow rates. The nozzle tip was, therefore, bathed in CO₂ at a very low horizontal flow rate (1 L/min), which successfully eliminated the erratic current behavior, presumably by preventing corona from developing. Due to the difference in density between air and CO₂, a small acceleration of the air in the vertical direction might result but this is expected to be negligible compared with the electrostatic acceleration forces. The PDPA analysis of the water spray revealed that the aerosol cone was populated mainly by droplets of between 8 and 12 μm diameter, however, there also existed a stream of much larger droplets of approximately 40 μm diameter along the axis with significantly lower velocities.

Despite the nonuniformity of the spray, it remained radially symmetric about the vertical axis. This is demonstrated in Fig. 4, in which the average droplet velocity and detection rate are plotted against distance from the origin along the X-axis at two different heights. The velocity measurements indicate that the water spray has a slight sideways inclination and the detection rate data indicates the extent of the expanding spray cone.

A set of power measurements was produced in exactly the same manner as the ethanol experiments. The distance from the 1.5 mm id nozzle to the counter electrode was 22 mm. The flow rate was set to 15 mL/h and the voltage across

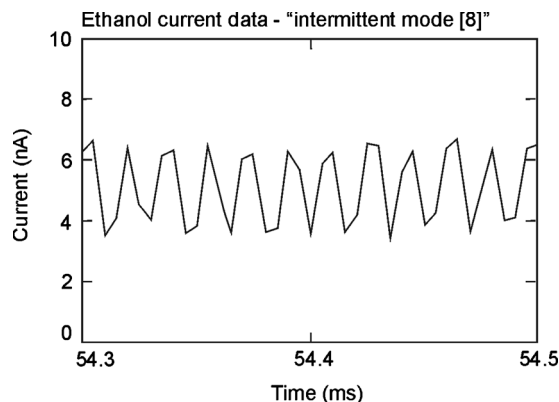


FIG. 2. Typical current signal during the ethanol EHDA experiments.

the electrodes was 9.2 kV. PDPA droplet size and velocity data was sampled at five downstream planes. Measurements were made at several locations in each horizontal plane, leading to the results presented in Table I. The measurable energy outputs are compared with the energy inputs in Table II and it is seen that the minimum estimate of the observed EHDA efficiency ranged from 2.96–9.04 $\pm 20\%$, which is depicted in Fig. 3(a) and represents another clear demonstration of energy gain.

C. Experimental data considerations

The most significant assumption on which this analysis rests is that droplet evaporation is negligible and the liquid flow rate through each measurement layer is equal to the initial flow leaving the nozzle. This is implied in the use of the constant k_z defined by Eq. (3). In order to assess the validity of this assumption, the average droplet diameter, d_z , was calculated for each measurement plane, z , for both the water and ethanol data. The results are presented in Table II and Fig. 3(b) in which the error bars denote \pm one standard deviation. In the case of ethanol, the droplets appear to slightly decrease in size as they descend, but for water, they appear to slightly increase. There is not enough data to predict a trend in either case. Given the experimental uncertainties, this data presents no evidence of significant droplet di-

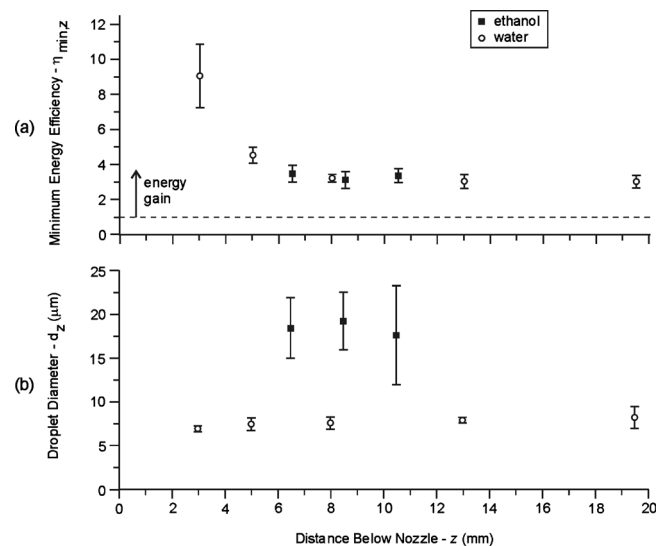


FIG. 3. Measured energy efficiency and average droplet diameter as a function of distance below nozzle.

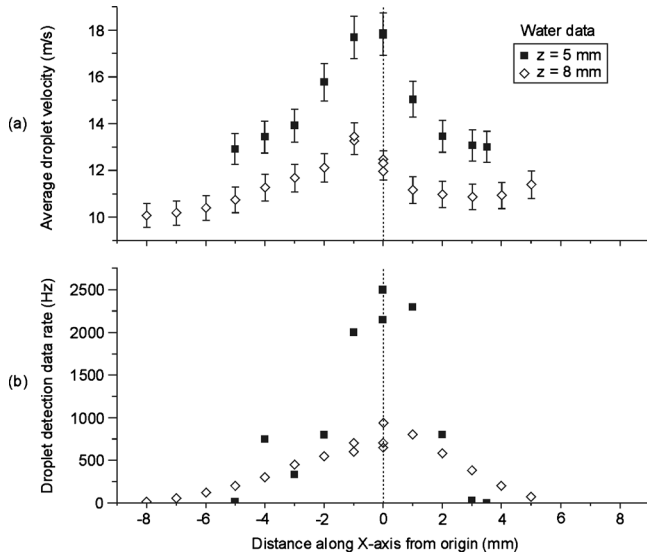


FIG. 4. Water droplet velocity and droplet detection rate along the X-axis at two heights, z .

ameter decrease with height. Further, if evaporation had a significant effect on our analysis, the measurements nearest the nozzle would be the least affected. However, Table II clearly demonstrates that the highest energy gain measurements are nearest the nozzle, where the least amount of evaporation can have occurred, and where the constant flow rate assumption is most accurate. Since there is no evidence of significant droplet evaporation as a function of height, the assumption of constant liquid volume flow through each layer which is equal to the nozzle flow rate is considered justified, validating the data handling methodology.

In both experiments, great care was taken to ensure that the electric field at the tip of the emitting nozzle was kept below the ionization threshold of the electrospray system because corona discharge would lead to electrical power being lost to the environment and not contributing to the creation and acceleration of the aerosol droplets. The applied voltage leading to this threshold is difficult to predict as it is a complex function of nozzle geometry, flow rate, background gas and the properties of the liquid itself. The evidence that all of the data presented here was taken below the ionization threshold was the low value of the dc current component. In both the water and ethanol experiments, for a pre-set flow rate, the voltage was raised slowly from zero while monitoring the current and visually inspecting the aerosol spray. For both liquids, during this voltage ramping, a sharp transition was observed at which the current levels increased from less than 20 nA to more than 100 nA accompanied by observable instability of the aerosol spray. This voltage value was noted and all measurements were performed significantly below this level. This distinct transition was taken to represent the measured ionization voltage

threshold at which high frequency (megahertz) corona discharges can occur. Below this threshold, any current oscillations can be considered to be due to low frequency pulsations in the geometry of the liquid emitting region.⁵ It is therefore, reasonable to assume that our measurement system with a 200 kHz sampling speed produces a true record of the dc and ac components of the EHDA current in the nozzle. It should be noted that in all cases a background current level was recorded with the full voltage impressed on the electrodes but no liquid flowing. This signal was very low but nevertheless the reported current signal was always the recorded signal corrected for the combination of background level and amplifier offset.

According to the classification of EHDA spraying modes in Ref. 8, the experiments presented here were all in the “intermittent” mode. This mode is typified by low voltage and low current, while nevertheless demonstrating regular emission time intervals, but with a fairly wide distribution of droplet sizes. One cannot therefore, assume the validity of the scaling laws^{8,9} that relate current, droplet size and other physical parameters corresponding to cone-jet mode EHDA spraying.

Thermal energy input was not considered in the analysis for two reasons. First, thermal energy is three-dimensional random Brownian motion and therefore, cannot cause the highly directional droplet trajectories that dominate the kinetic energy term, P_{KIN} . Second, the only other observable energy output that could have been affected by thermal energy input would be the surface energy term, P_{SURF} , which would be affected if significant evaporation or condensation was occurring. However, the droplet diameter evidence in Fig. 3(b) indicates that there is no detectable evaporation or condensation and therefore, thermal energy plays no part in the energy balance described by Eq. (11).

When evaluating the statistical significance of the data presented in Tables I and II, it should be realized that $N_{i,j}$, is different for each observation period. In the central regions, $N_{i,j} \sim 20\,000\text{--}30\,000$ droplets, but in the outer zones $N_{ij} \sim 300$ droplets. M_i , the number of measurement intervals in region, i , also differed with location in the spray cone. Toward the edge of the cone, only a single observation period was used while in the central areas up to seven measurement intervals were performed in one or more locations within a single region.

D. Error analysis

The accuracy of the efficiency results, $(\Delta \eta_{\min,z} / \eta_{\min,z})$, listed in Table II and depicted in Fig. 3(a) depends on the uncertainty in the individual parameter measurements and the validity of the assumptions inherent in the statistical sampling method. Applying basic error propagation rules to Eq. (11) allows the relative efficiency uncertainty to be written as

$$\left(\frac{\Delta \eta_{\min,z}}{\eta_{\min,z}} \right) = \sqrt{\frac{(\Delta P_{KIN,z})^2 + (\Delta P_{SURF,z})^2}{(P_{KIN,z} + P_{SURF,z})^2} + \frac{(\Delta P_{ELEC})^2 + (\Delta P_{PUMP})^2 + (\Delta P_{GRAV,z})^2 + (\Delta P_{SURF,I})^2}{(P_{ELEC} + P_{PUMP} + P_{GRAV,z} + P_{SURF,I})^2}}, \quad (12)$$

where the ΔP terms represent the absolute uncertainty of the corresponding power terms and are defined by Eqs. (A14), (A16), (A19), and (A21)–(A23) derived in the Appendix. Equation (12) is used to calculate the relative uncertainties listed in the last column of Table II and depicted by the error bars in Fig. 3(a).

The largest absolute uncertainty in the estimation of the energy input occurs in the measurement of the electrical power. Nevertheless, it is demonstrated in the Appendix that the uncertainty in P_{ELEC} is less than 3.5%. The TSI-Aerometrics PDPA system is reported to give velocity measurements with an error of <1% and droplet sizes to within 0.5 μm . Using these ranges combined with the analysis presented in the Appendix leads to overall efficiency uncertainties of less than 3.5%. This is, however, based on the assumption that droplet velocities and diameters are constant in a given measurement region, (i, z). In reality, both the droplet velocities (see Fig. 4) and diameters vary as a function of radial position in the spray and therefore, the data will probably vary even within a single measurement region, leading to an increased uncertainty in the efficiency results. Precise quantification of these radially dependent uncertainties would be very complex due to a large number of influencing factors. Therefore, a conservative approach was adopted in which significantly larger values for velocity and diameter uncertainty were applied to the error analysis which remained constant for all measurements with each liquid. It was found that velocity data from any particular measurement region (i, z) varied within a 10% range around the measured value. Therefore, a 10% uncertainty in the individual droplet velocity values was used in the error analysis which was significantly higher than the manufacturer quoted measurement error of the PDPA system. More importantly, the value of the efficiency uncertainty given by Eq. (12) was dominated by the uncertainty of the droplet diameter within a particular measurement region (i, z). Inspection of the distribution of diameter measurements demonstrated that the uncertainty of the region specific ethanol droplet diameter data was $\pm 2 \mu\text{m}$ and $\pm 1 \mu\text{m}$ for the water data. According to the analysis presented in the Appendix, this leads to a relative uncertainty as high as 23% for the kinetic power and 29% for the surface power terms for the water results at $z = 3 \text{ mm}$. However, for the water measurements at other heights, the two output power terms had relative errors of 17% or less and the relative error of these terms with the ethanol data was 20% or less.

IV. THEORETICAL CONSIDERATIONS

A. Stored bond energy in liquids

All chemical bonds including intermolecular bonds occur as a result of the classical and nonclassical electric and magnetic interactions between the subatomic particles that make up the two bonding entities.¹⁰ Some of the subatomic particle interactions result in attractive forces while others cause repulsion. In a stable bond, the net forces of attraction and repulsion are equal and opposite when the entities are at their equilibrium separation distance. All of the attractive forces can be grouped together and described by a potential

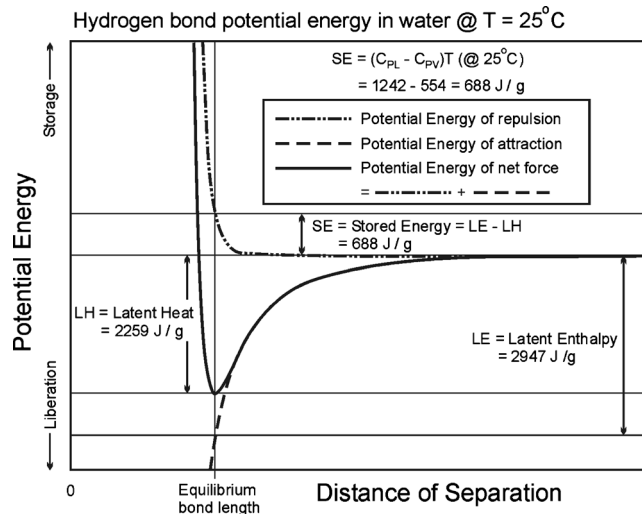


FIG. 5. Depiction of the potential energy curves describing the hydrogen bond in liquid water.

energy of attraction. The same can be done for the forces of repulsion. The sum of these two potential energies is often described as the potential energy profile of a bond. Three such curves are depicted in Fig. 5.

Figure 5 is a two-dimensional oversimplification of the potential energy profile involved in a hydrogen bond since water and ethanol molecules are not spherically symmetric and the actual potentials depend highly on the location and orientation of neighboring molecules. Nevertheless, the average empirically determined values for bulk water at 25 °C are presented in Fig. 5 since it is the most accurately measured liquid due to its crucial importance for life and earth sciences.

The least well discussed quantity in this model is the *latent enthalpy* (LE), which is liberated as the entities approach each other. It represents the reorganisation of the electron structures of the bonding pair and is therefore, not directly measurable as heat and consequently not listed in data tables. As the LE is liberated during bond formation, it is transformed into two different forms; the *latent heat of vaporisation* (LH) and *stored energy of repulsion* (SE).

$$LE = LH + SE. \quad (13)$$

If the LH is not released to the environment during their approach, the bond cannot occur and the entities simply bounce apart. However, if the pair are able to shed the LH, then a bond is formed, trapping the SE as energy of repulsion, like a compressed spring. This stored energy is the most likely source of the gain observed in the EHDA experiments and pulsed water arcs.

When intermolecular bonds are broken by thermal forces, a quantity of heat is absorbed from the environment, which has been measured and tabulated as bond dissociation energy and is equal to LH. It is, however, not detectable by calorimetry that the stored energy, SE, is also a component of the net energy required to break the bond with heat. Thermal rupture of a bond is relatively slow, occurring as a consequence of many external collisions. The SE is therefore, re-

leased gradually, like weakening fingers slowly releasing the energy stored in a compressed spring in a controlled manner.

In contrast, highly localized and directional nonthermal forces such as electrostatic force in the EHDA experiments or electrodynamic force in pulsed arc experiments are expected to break intermolecular bonds more efficiently since all of the force can be applied along a single axis which represents the consequent direction of acceleration. The process is also probably more rapid than thermal dissociation as it does not require multiple random collisions. The experimental consequence of application of this type of force is the apparent measurable release of the SE, leading to quantifiable energy gain as described in this paper and elsewhere.^{1,2} This nonthermal mechanism is analogous to the energy stored in a spring, initially compressed by two plates held together by a ratchet system, but then explosively released by an efficient (low energy) flick of the ratchet trigger.

Most commonly applied in atmospheric meteorology, the Kirchoff equation¹¹ relating LH to the temperature, T and C_{PV} and C_{PL} , the specific heat capacities at constant pressure of vapor and liquid, respectively, is

$$\frac{dLH}{dT} = C_{PV} - C_{PL} \quad \text{or} \quad LH = LH_0 - (C_{PL} - C_{PV})T. \quad (14)$$

A paper exploring the conservation of energy during condensation¹² examined the meaning of the constant, LH_0 , and proposed a variant of Eq. (14) as

$$LE = LH + (C_{PL} - C_{PV})T. \quad (15)$$

The author claimed that the second term on the right hand side of Eq. (15) “is entirely absorbed by the liquid water in order to ensure equilibrium in the postcondensation system. In the case of evaporation, this same energy difference would be liberated.” Comparison of Eqs. (13) and (15) in conjunction with the quotation above support the interpretation of the energy bands in Fig. 5 and allows a prediction of the SE in the intermolecular bond as

$$SE = (C_{PL} - C_{PV})T. \quad (16)$$

In general the specific heat capacities of liquid and vapor have a small temperature dependence and thus the stored energy is a slightly nonlinear function of temperature. If we use the tabulated specific heat capacities for liquid water and water vapor at 25 °C as shown in Fig. 5, the stored energy in hydrogen bonds in water is 688 J/g or J/cm³.

In a similar manner using data for the specific heats of ethanol liquid and vapor in Eq. (16) yields a stored bond energy of 155 J/g or 122 J/cm³ at 25 °C. The stored bond energy density of ethanol is expected to be lower than water as it forms fewer hydrogen bonds per molecule due to possessing only one hydrogen atom with sufficient charge deficiency. In contrast, water has two hydrogen atoms available for hydrogen bonding and is a smaller molecule, and therefore, stores 5.6 times more bond energy per unit volume. All liquids are held together by some form of intermolecular bonding network which must store energy and thus an energy gain should be observable with all liquids to a greater or

lesser extent. However, water, with its high surface tension, is likely to be the largest store of this intermolecular energy due to its high hydrogen bond density.

These results reveal that during the EHDA water experiments, with a flow rate of 15 mL/h, the stored energy in the bulk liquid represents about 2.9 W of potential power. However, at 3 mm below the nozzle, only 1.1 mW of kinetic and surface energy power has been gained. The very low percentage of conversion of stored energy to kinetic and surface energy (0.04%) is primarily due to the very small percentage of the total number of hydrogen bonds that are broken. This implies that more energy will be produced by techniques that divide the liquid into smaller droplets.

B. The renewable nature of intermolecular bond energy

Traditional chemical energy sources rely on conversion of a fuel into another substance of no further use. In contrast, the EHDA and water arc mechanisms of liberating bond energy do not change the chemical molecules in the fuel. They only convert bulk liquid into droplets. In both of these types of experiment, the micron scale droplets are seen to readily convert back to bulk liquid as soon as, or even before, they collect on a surface from which they can extract the heat required to restore their electron structure. This cycle of chemical bond breaking and reforming is therefore, renewable. If a device is developed that can harness the kinetic energy of the liquid while it is in high velocity droplet form, then this represents a novel energy generator, driven by a renewable energy source. If the liquid in such a device was encapsulated and continually recycled, then the ultimate energy source would be the atmospheric heat required to supply energy to the surface at which the droplets agglomerate back to bulk liquid.

Intermolecular bond formation in a liquid usually produces heat and does not consume it as just described. However, the unusual electron structures of the liquid droplets produced by the EHDA and water arc experiments presumably require thermal energy to be added to restore them to their normal unbonded state. The combined electron structure of two unbonded molecules is clearly in a higher energy state than the electron structure of a bonded pair and the difference between these two states is the LE. In thermal bond dissociation, heat is gradually injected into the electron structure and when combined with the SE, eventually the electrons find themselves in an unbonded configuration and the entities separate. If, however, the bond is broken rapidly by a directed electric force, the SE can be released as kinetic energy, leaving the entities separated but their electron structures in lower than normal energy configurations. These droplets may then have high kinetic energy, available for harnessing, but their electron structure still requires energy (heat) to recover the normal unbonded configuration. Therefore, the EHDA and water arc experiments represent two mechanisms of extracting some of the energy, which is normally transferred as heat every time hydrogen bonds are formed and broken, and converting it into useful directed kinetic energy which can potentially be used for electricity generation. In an enclosed liquid system, any energy which

is extracted by such a generator will eventually be returned into the liquid by heat absorbed from the atmosphere, making this a novel renewable energy generating system.

V. SUMMARY AND CONCLUSIONS

Recent EHDA electrospray experiments using both ethanol and water have revealed energy gains when comparing the kinetic and surface tension energy outputs with the electrical, gravitational, and pump energy inputs. Without being able to measure energy lost to air friction, the energy gain measurement was only a conservative estimate, but nevertheless ranged from 305%–341% for an ethanol aerosol and from 296%–904% for water. The uncertainties for these efficiency measurements are calculated by the method discussed in the Appendix and are presented in Table II and Fig. 3(a). Energy conservation requires that these results can only be possible if a source of stored energy is being released. The most likely mechanism is considered to be energy of repulsion stored in the hydrogen bonding network in the liquid prior to breaking into droplets, which is entirely consistent with conventional bonding theory. Therefore, these electrospray experiments have demonstrated for the first time that renewable energy, stored in liquids, can be continuously converted into mechanical energy.

While this experiment only produced energy gains in the hundreds of microwatts, it represents the basis of a potential electricity generator driven by a renewable source which could have a significant impact on meeting our future energy and environmental needs. The next type of experiments which are hoped to lead toward possible generator technologies will probably include innovations such as the incorporation of thinner and multiple nozzles or roughened surfaces. It is hoped that this type of relatively simple experiment will also be attempted in other laboratories to gain corroboration and raise awareness of the discovery of a new field of energy research.

ACKNOWLEDGMENTS

We would like to acknowledge the interest and support of WETSUS, Centre of Excellence for Sustainable Water Technology, Leeuwarden, Netherlands, who provided the funding and international coordination required to perform these experiments. We also appreciate the moral support and many important discussions with Dr. Peter Graneau.

APPENDIX: DERIVATION OF THE UNCERTAINTY VALUES USED IN THE ERROR ANALYSIS

The measurements performed to determine the conservative estimate of the efficiency, $\eta_{\min,z}$, of the EHDA liquid to droplet conversion process all possess a level of uncertainty. These inaccuracies propagate through the calculations and result in the uncertainty of the determined efficiency as described by Eq. (12). Here, expressions for each of the uncertainty terms in Eq. (12) are derived and justified.

1. Measurement accuracies

a. PDPA measurements

The accuracy of the PDPA measurements is specified by the manufacturer, implicitly assuming a correctly aligned and configured system. The droplet velocity measurements are expected to have an accuracy of $\leq 1\%$ and the diameter measurements are expected to be within $\pm 0.5 \mu\text{m}$. Therefore,

$$\Delta d_{j,l} = 0.5 \mu\text{m} \quad \text{and} \quad \frac{\Delta v_{v,j,l}}{v_{v,j,l}} = \frac{\Delta v_{h,j,l}}{v_{h,j,l}} = 0.01 = \frac{\Delta v}{v}. \quad (\text{A1})$$

b. Potential difference

The potential difference applied between the nozzle and the planar electrode was determined by reading the value from the display on the dedicated power supply. The reading resolution on the digital display was $\pm 0.05 \text{ kV}$ and the power supply was specified by the manufacturer to have an accuracy of $< \pm 0.2\%$ of the nominal output value. The maximum output voltage of the power supply is 20 kV and therefore, the uncertainty is dominated by the reading resolution, leading to $\Delta V_{PS} = 50 \text{ V}$.

c. Current measurement

The current through the EHDA system was measured by monitoring the voltage across a known shunt resistance. An A/D-converter reproduced the signal in digital form, enabling storage and postprocessing. The shunt resistance produces thermal noise in the measurement system while the A/D-converter is limited by resolution. In most cases, the signal is amplified before it is digitised.

Resistor and amplifier accuracy. The measurable thermal noise of a resistor is a function of R , the resistance value, k_B , the Boltzmann constant, f_{BW} , the bandwidth of the system and T , the temperature of the resistor which is assumed to be equal to the background temperature. If the voltage signal, proportional to the system current, as well as the unavoidable thermal noise are amplified by the INA110KP integrated circuit with a gain, G , then the root mean squared noise term at the amplifier output, $\tilde{V}_{n,\text{rms}}$, is given by

$$\tilde{V}_{n,\text{rms}} = G\sqrt{4k_BTRf_{BW}}. \quad (\text{A2})$$

The absolute uncertainty of the magnitude of the amplified noise signal is given by

$$\begin{aligned} (\Delta \tilde{V}_{n,\text{RMS}})^2 &= \left(\frac{\partial \tilde{V}_{n,\text{RMS}}}{\partial R} \right)^2 (\Delta R)^2 + \left(\frac{\partial \tilde{V}_{n,\text{rms}}}{\partial T} \right)^2 (\Delta T)^2 \\ &+ \left(\frac{\partial \tilde{V}_{n,\text{rms}}}{\partial G} \right)^2 (\Delta G)^2 + \left(\frac{\partial \tilde{V}_{n,\text{rms}}}{\partial k_B} \right)^2 (\Delta k_B)^2 \\ &+ \left(\frac{\partial \tilde{V}_{n,\text{rms}}}{\partial f_{BW}} \right)^2 (\Delta f_{BW})^2. \end{aligned} \quad (\text{A3})$$

Referring to Eq. (A2), resolving the partial derivatives and rearranging terms yields

$$\begin{aligned}
(\Delta \tilde{V}_{n,rms})^2 &= \left(\frac{1}{2} \tilde{V}_{n,rms}\right)^2 \left[\left(\frac{\Delta R}{R}\right)^2 + \left(\frac{\Delta T}{T}\right)^2 + 4\left(\frac{\Delta G}{G}\right)^2 \right. \\
&\quad \left. + \left(\frac{\Delta k_B}{k_B}\right)^2 + \left(\frac{\Delta f_{BW}}{f_{BW}}\right)^2 \right] \\
&\approx \left(\frac{1}{2} \tilde{V}_{n,rms}\right)^2 \left[\left(\frac{\Delta R}{R}\right)^2 + \left(\frac{\Delta T}{T}\right)^2 + 4\left(\frac{\Delta G}{G}\right)^2 \right]
\end{aligned} \tag{A4}$$

The Boltzmann constant is considered fixed and the bandwidth is determined by the data acquisition frequency which is considered to be very accurate and therefore, has a much lower relative uncertainty than the resistance, gain and temperature values. The manufacturer of the amplifier circuit quotes a gain dependent uncertainty which has a maximum value of $\Delta G/G \leq 0.005$. The 99.7 k Ω . shunt resistance had a 1% tolerance therefore, $\Delta R/R = 0.01$. The temperature uncertainty was less than that for the resistance and gain, $\Delta T/T < 0.005$.

A/D conversions. For the A/D conversion, an oscilloscope recorded the output of a 12-bit IO card. Even though the oscilloscope could only resolve eight-bit values, its flexibility assisted the selection of the most appropriate measurement range which increased the accuracy. The measurement ranges of the IO card were adjusted between measurement intervals to optimise the acquisition resolution. Hence it is assumed that all resistor voltage measurements, V , were obtained with at least seven-bit resolution. Hence the uncertainty of the voltage measurements due to the A/D conversion, ΔV_{AD} , are therefore, assumed to be given by

$$\frac{\Delta V_{AD}}{V} = \frac{1}{2^7} = 7.8 \times 10^{-3}. \tag{A5}$$

Current measurement accuracy. A conservative estimate of the voltage measurement accuracy, ΔV , is determined by the larger of the A/D conversion or noise amplification uncertainties as expressed as

$$\Delta V = \max\{\Delta V_{AD} \text{ or } (\tilde{V}_{n,rms} + \Delta \tilde{V}_{n,rms})\}. \tag{A6}$$

The electric current value is finally determined using Ohm's law, ($V=IR$), resulting in an absolute uncertainty in the current measurements, ΔI , given by

$$\begin{aligned}
(\Delta I)^2 &= \left(\frac{\partial I}{\partial V}\right)^2 (\Delta V)^2 + \left(\frac{\partial I}{\partial R}\right)^2 (\Delta R)^2 \\
&= \frac{1}{R^2} (\Delta V)^2 + I^2 \left(\frac{\Delta R}{R}\right)^2.
\end{aligned} \tag{A7}$$

The relative uncertainty in the current measurement is therefore,

$$\left(\frac{\Delta I}{I}\right)^2 = \left(\frac{\Delta V}{V}\right)^2 + \left(\frac{\Delta R}{R}\right)^2. \tag{A8}$$

Using Eqs. (A2) and (A4)–(A6) and the most conservative relative uncertainty estimates for R , G , and T leads to the conclusion that $\Delta I/I = 2.5\%$ for ethanol and $\Delta I/I = 1.3\%$ for the water measurements.

d. Liquid flow rate

The liquid flow rate was controlled by a PHD 2000 syringe pump with a specified accuracy of $\pm 1\%$, therefore, $\Delta f/f = 0.01$, where f and Δf are, respectively, the liquid flow rate and its absolute uncertainty.

e. Capillary diameter

The internal diameter of the steel capillary nozzle, $d_{cap} = 1.5$ mm, was taken from the manufacturer's documentation with a specified absolute accuracy of $\Delta d_{cap} = 0.005$ mm, resulting in a relative accuracy of $\pm 0.3\%$.

f. Vertical positioning

The EHDA system (nozzle and planar electrode) were fixed together and mounted on a three-dimensional translation stage in order to be able to make PDPA measurements at different positions in the electro spray cone. In the vertical direction, the position of the translation system could be read on a micrometer dial to an accuracy of ± 10 μm . This system was also used to determine the origin of the vertical positions at the lowest point of the capillary. Hence the absolute error in the difference in height between the nozzle tip and the PDPA measurement position, z , follows from $\Delta z = \sqrt{(10^{-5})^2 + (10^{-5})^2} = 14$ μm .

2. Accuracy of the power outputs

Expressions for the uncertainty of the power outputs are derived in Secs. 2 a–2 f based on Eqs. (1)–(6) and measurement techniques developed in Sec. II A.

a. Measured liquid volume

The detected liquid flow rate in modeling region, i , at measurement height, z , is defined as $\Phi_{i,z}$, expressed as Eq. (1). Measurement intervals were all several minutes long and were, therefore, timed with high accuracy. Consequently, the uncertainty of $t_{i,j}$ is not included in the error analysis. The number of detected droplets is also known precisely. The only partial derivative that will therefore, be required to assess the uncertainty in the measured flow rate is

$$\frac{\partial \Phi_{i,z}}{\partial d_{j,l}} = \frac{\pi}{6M_i} \left(\frac{3d_{j,l}^2}{t_{i,j}} \right). \tag{A9}$$

The absolute error in the detected flow rate can therefore, be written as

$$\begin{aligned}
(\Delta \Phi_{i,z})^2 &= \sum_{j=1}^{M_i} \sum_{l=1}^{N_{i,j}} \left(\frac{3\pi d_{j,l}^2}{6M_i t_{i,j}} \right)^2 (\Delta d_{j,l})^2 \\
&= \left(\frac{\pi}{2M_i} \right)^2 \sum_{j=1}^{M_i} \left(\frac{1}{t_{i,j}} \right)^2 \sum_{l=1}^{N_{i,j}} d_{j,l}^4 (\Delta d_{j,l})^2.
\end{aligned} \tag{A10}$$

In Sec. 1 a, it was argued that due to variability within the spray, the relative uncertainty in the droplet measurement was given by Eq. (A1), hence Eq. (A10) can be solved for $\Delta \Phi_{i,z}$ by computer for each i, z region.

b. Measurement area proportionality constant, k_z

The height dependent constant, k_z , required to relate the measured flow rate, $\Delta\Phi_{i,z}$, to the estimated total flow rate through a region, i, z is given by Eq. (3). The absolute error in k_z can therefore, be expressed as

$$\begin{aligned} (\Delta k_z)^2 &= \left(\frac{\partial k_z}{\partial f}\right)^2 (\Delta f)^2 + \sum_{i=0}^n \left(\frac{\partial k_z}{\partial \Phi_{i,z}}\right)^2 (\Delta \Phi_{i,z})^2 \\ &= \left(\frac{f}{\sum_{i=0}^n \frac{A_i}{A_{tot}} \Phi_{i,z}}\right)^2 \left(\frac{\Delta f}{f}\right)^2 \\ &\quad + \sum_{i=0}^n \left[-\left(\frac{A_i}{A_{tot}}\right) \frac{f}{\left(\sum_{i=0}^n \frac{A_i}{A_{tot}} \Phi_{i,z}\right)^2} \right]^2 (\Delta \Phi_{i,z})^2. \end{aligned} \quad (\text{A11})$$

The expression for the absolute uncertainty in the k_z measurement can be solved by computer with knowledge of the individual areas, A_i , the uncertainty of the total flow rate from Sec. 1 d and Eqs. (1), (A1), and (A10).

c. Kinetic power in a single region, $P_{KIN,meas,i,z}$

The kinetic power measured in a region, i, z , is defined as $P_{KIN,meas,i,z}$ in Eq. (2). Consequently, the absolute uncertainty in this measurement is given by

$$\begin{aligned} (\Delta P_{KIN,meas,i,z})^2 &= \sum_{j=1}^{M_i} \sum_{l=1}^{N_{i,j}} \left[\left(\frac{\partial P_{KIN,meas,i,z}}{\partial d_{j,l}}\right)^2 (\Delta d_{j,l})^2 \right. \\ &\quad + \left(\frac{\partial P_{KIN,meas,i,z}}{\partial v_{v,j,l}}\right)^2 (\Delta v_{v,j,l})^2 \\ &\quad \left. + \left(\frac{\partial P_{KIN,meas,i,z}}{\partial v_{h,j,l}}\right)^2 (\Delta v_{h,j,l})^2 \right]. \end{aligned} \quad (\text{A12})$$

Both the vertical and horizontal velocities are considered to have the same measured uncertainty due to the variability of the spray as discussed in Sec. 1 a. Therefore, by taking the partial derivatives in Eq. (A12), rearranging the terms and including Eq. (A1) yields

$$\begin{aligned} (\Delta P_{KIN,meas,i,z})^2 &= \left(\frac{\pi\rho}{12M_i}\right)^2 \sum_{j=1}^{M_i} \left\{ \frac{1}{t_{i,j}^2} \sum_{l=1}^{N_{i,j}} [9d_{j,l}^4 (v_{v,j,l}^2 \right. \\ &\quad + v_{h,j,l}^2) (\Delta d_{j,l})^2] \\ &\quad \left. + \left[4d_{j,l}^6 (v_{v,j,l}^4 + v_{h,j,l}^4) \left(\frac{\Delta v}{v}\right)^2 \right] \right\}, \end{aligned} \quad (\text{A13})$$

which can be solved by computer for all measurement regions, i, z .

d. Total kinetic power, $P_{KIN,z}$

The total kinetic power flowing through the horizontal plane at height, z , is obtained by summing the measured kinetic powers in each region, i , and taking into account the

scaling factor, k_z , according to Eq. (4). The absolute uncertainty in this measurement is therefore, expressed as

$$\begin{aligned} (\Delta P_{KIN,z})^2 &= \left(\frac{\partial P_{KIN,z}}{\partial k_z}\right)^2 (\Delta k_z)^2 \\ &\quad + \left(\frac{\partial P_{KIN,z}}{\partial P_{KIN,meas,i,z}}\right)^2 (\Delta P_{KIN,meas,i,z})^2 \\ &= \left(\sum_{i=0}^n \frac{A_i}{A_{tot}} P_{KIN,meas,i,z}\right)^2 (\Delta k_z)^2 \\ &\quad + \sum_{i=0}^n \left[\left(\frac{A_i}{A_{tot}} k_z\right)^2 (\Delta P_{KIN,meas,i,z})^2 \right]. \end{aligned} \quad (\text{A14})$$

By combining results from solutions of Eqs. (3), (4), (A11), and (A13) and knowledge of the areas of the i measurement sectors, a computer used Eq. (A14) to calculate the absolute uncertainty in the total kinetic power flow measurement through the plane, z .

e. Surface power in a measurement region, $P_{SURF,meas,i,z}$

The surface power measured in a region, i, z , is defined as $P_{SURF,meas,i,z}$ in Eq. (5). Consequently, the absolute uncertainty in this measurement is given by

$$\begin{aligned} (\Delta P_{SURF,meas,i,z})^2 &= \left(\frac{\partial P_{SURF,meas,i,z}}{\partial d_{j,l}}\right)^2 (\Delta d_{j,l})^2 \\ &= \left(\frac{2\pi\sigma}{M_i}\right)^2 \left(\sum_{j=1}^{M_i} \frac{1}{t_{i,j}} \sum_{l=1}^{N_{i,j}} d_{j,l}\right)^2 (\Delta d_{j,l})^2. \end{aligned} \quad (\text{A15})$$

Using Eq. (A1), Eq. (A15) can be solved for all measurement regions, i, z .

f. Total surface power, $P_{SURF,z}$

The total surface power flowing through the horizontal plane at height, z , is obtained by summing the measured surface powers in each region, i , taking into account the scaling factor, k_z , according to Eq. (6). The absolute uncertainty in this measurement is, therefore, expressed as

$$\begin{aligned} (\Delta P_{SURF,z})^2 &= \left(\frac{\partial P_{SURF,z}}{\partial k_z}\right)^2 (\Delta k_z)^2 \\ &\quad + \left(\frac{\partial P_{SURF,z}}{\partial P_{SURF,meas,i,z}}\right)^2 (\Delta P_{SURF,meas,i,z})^2 \\ &= \left(\sum_{i=0}^n \frac{A_i}{A_{tot}} P_{SURF,meas,i,z}\right)^2 (\Delta k_z)^2 \\ &\quad + k_z^2 \sum_{i=0}^n \left[\left(\frac{A_i}{A_{tot}}\right)^2 (\Delta P_{SURF,meas,i,z})^2 \right]. \end{aligned} \quad (\text{A16})$$

By combining results from solutions of Eqs. (3), (6), (A11), and (A15) and knowledge of the areas of the i measurement sectors, a computer used Eq. (A16) to calculate the absolute uncertainty in the total surface power flow measurement through the plane, z .

3. Accuracy of the power inputs

Expressions for the uncertainty of the power inputs are derived in Secs. 3 a–3 d based on Eqs. (7)–(10) and measurement techniques developed in Sec. II B. The material and physical constants are assumed to be known very accurately with respect to the measurements and as a result they are not considered as variables in the error analysis.

a. Electrical input power, P_{ELEC}

The electrical power input term is given by Eq. (7). The accuracy of the voltage term, V_{PS} , is discussed in Sec. 1 b. I_{av} is the arithmetic mean of the individual sampled current values for which the accuracy is discussed in Sec. 1 c. The absolute uncertainty of the average current, ΔI_{av} , is given by

$$(\Delta I_{av})^2 = \sum_{i=1}^n \left[\left(\frac{1}{n} \right)^2 (\Delta I)^2 \right]. \quad (\text{A17})$$

Therefore,

$$\Delta I_{av} = \frac{1}{\sqrt{n}} \Delta I, \quad (\text{A18})$$

where ΔI is calculated from the results presented in Sec. 1 c and n is the number of samples used to determine the average. It is therefore, clear that $\Delta I_{av} = \Delta I$ provides a conservative estimate of ΔI_{av} . From Eq. (7), it follows that the absolute error ΔP_{ELEC} , is given by

$$\begin{aligned} (\Delta P_{ELEC})^2 &= \left(\frac{\partial P_{ELEC}}{\partial I_{av}} \right)^2 (\Delta I_{av})^2 + \left(\frac{\partial P_{ELEC}}{\partial V_{PS}} \right)^2 (\Delta V_{PS})^2 \\ &= I_{av}^2 V_{PS}^2 \left(\left(\frac{\Delta I_{av}}{I_{av}} \right)^2 + \left(\frac{\Delta V_{PS}}{V_{PS}} \right)^2 \right), \end{aligned} \quad (\text{A19})$$

which can be solved by applying data from Sec. 1 b. The relative error is defined by

$$\frac{\Delta P_{ELEC}}{P_{ELEC}} = \sqrt{\left(\frac{\Delta I_{av}}{I_{av}} \right)^2 + \left(\frac{\Delta V_{PS}}{V_{PS}} \right)^2}. \quad (\text{A20})$$

For the results described in this paper, and using the conservative assumption that $\Delta I_{av} = \Delta I$, Eq. (A20) predicts relative uncertainties in the electrical power measurement of 3.5% and 1.5% for the ethanol and water data, respectively.

b. Pump input power, P_{PUMP}

The kinetic power added to the system by the syringe pump is given by Eq. (8). The absolute error, ΔP_{PUMP} is thus given by

$$\begin{aligned} (\Delta P_{PUMP})^2 &= \left(\frac{8\rho}{\pi^2} 3 \frac{f^2}{d_{cap}^4} \right)^2 (\Delta f)^2 \\ &+ \left(\frac{8\rho}{\pi^2} (-4) \frac{f^3}{d_{cap}^5} \right)^2 (\Delta d_{cap})^2. \end{aligned} \quad (\text{A21})$$

c. Gravitational power, P_{GRAV}

The kinetic power gained by the water spray by gravitational force, measured at a height z , $P_{GRAV,z}$, is described by

Eq. (9). The values of g , the gravitational constant and ρ , the liquid density are considered to be tabulated constants and therefore, known with full precision. Consequently, the absolute uncertainty in the gravitational power measurement is given by

$$\begin{aligned} (\Delta P_{GRAV,z})^2 &= \left(\frac{\partial P_{GRAV,z}}{\partial f} \right)^2 (\Delta f)^2 + \left(\frac{\partial P_{GRAV,z}}{\partial z} \right)^2 (\Delta z)^2 \\ &= (g\rho z)^2 (\Delta f)^2 + (fg\rho)^2 (\Delta z)^2. \end{aligned} \quad (\text{A22})$$

d. Surface energy input power, $P_{SURF,I}$

The surface tension energy flowing out of the nozzle prior to breaking up into droplets is defined as $P_{SURF,I}$, given by Eq. (10). The absolute uncertainty in the surface energy input power can therefore, be expressed as

$$\begin{aligned} (\Delta P_{SURF,I})^2 &= \left(\frac{\partial P_{SURF,I}}{\partial f} \right)^2 (\Delta f)^2 + \left(\frac{\partial P_{SURF,I}}{\partial d_{cap}} \right)^2 (\Delta d_{cap})^2 \\ &= \left(\frac{6\sigma}{d_{cap}} \right)^2 (\Delta f)^2 + \left(\frac{6\sigma f}{d_{cap}^2} \right)^2 (\Delta d_{cap})^2. \end{aligned} \quad (\text{A23})$$

4. Accuracy of the conservative efficiency estimate, $\eta_{\min,z}$

A minimum estimate of the efficiency of the conversion from liquid to aerosol spray, based on measurements at a height, z , and expressed as a percentage is given by Eq. (11). The various components of this equation as well as the absolute value of their uncertainties have all been assessed in previous sections. The absolute error in this conservative estimate of the system efficiency is given by

$$\begin{aligned} (\Delta \eta_{\min,z})^2 &= \left(\frac{\partial \eta_{\min,z}}{\partial P_{KIN,z}} \right)^2 (\Delta P_{KIN,z})^2 \\ &+ \left(\frac{\partial \eta_{\min,z}}{\partial P_{SURF,z}} \right)^2 (\Delta P_{SURF,z})^2 \\ &+ \left(\frac{\partial \eta_{\min,z}}{\partial P_{ELEC}} \right)^2 (\Delta P_{ELEC})^2 \\ &+ \left(\frac{\partial \eta_{\min,z}}{\partial P_{PUMP}} \right)^2 (\Delta P_{PUMP})^2 \\ &+ \left(\frac{\partial \eta_{\min,z}}{\partial P_{GRAV,z}} \right)^2 (\Delta P_{GRAV,z})^2 \\ &+ \left(\frac{\partial \eta_{\min,z}}{\partial P_{SURF,I}} \right)^2 (\Delta P_{SURF,I})^2. \end{aligned} \quad (\text{A24})$$

Referring to Eq. (11) and taking the partial derivatives and rearranging terms yields

$$(\Delta \eta_{\min,z})^2 = \frac{(\Delta P_{KIN,z})^2 + (\Delta P_{SURF,z})^2}{(P_{ELEC} + P_{PUMP} + P_{GRAV,z} + P_{SURF,I})} + \eta_{\min,z}^2 \left(\frac{(\Delta P_{ELEC})^2 + (\Delta P_{PUMP})^2 + (\Delta P_{GRAV,z})^2 + (\Delta P_{SURF,I})^2}{(P_{ELEC} + P_{PUMP} + P_{GRAV,z} + P_{SURF,I})^2} \right). \quad (\text{A25})$$

Taking the square root of the quotient of Eq. (A25) divided by Eq. (11) yields Eq. (12) which was used to calculate the relative uncertainties of the minimum efficiency measurement quoted in Table II and depicted in Fig. 3(a).

¹G. Hathaway, P. Graneau, and N. Graneau, *J. Plasma Phys.* **60**, 775 (1998).

²P. Graneau, N. Graneau, G. Hathaway, and R. L. Hull, *J. Plasma Phys.* **63**, 115 (2000).

³R. P. A. Hartman, D. J. Brunner, M. A. Camelot, J. C. M. Marijnissen, and B. Scarlett, *J. Aerosol Sci.* **31**, 65 (2000).

⁴G. Taylor, *Proc. R. Soc. London* **A280**, 383 (1964).

⁵I. Marginean, L. Parvin, L. Heffernan, and A. Vertes, *Anal. Chem.* **76**, 4202 (2004).

⁶L. Parvin, M. C. Galicia, J. M. Gauntt, L. M. Carney, A. B. Nguyen, E. Park, L. Heffernan, and A. Vertes, *Anal. Chem.* **77**, 3908 (2005).

⁷K. Tang and A. Gomez, *J. Colloid Interface Sci.* **175**, 326 (1995).

⁸M. Cloupeau and B. Prunet-Foch, *J. Aerosol Sci.* **25**, 1021 (1994).

⁹R. P. A. Hartman, D. J. Brunner, D. M. A. Camelot, J. C. M. Marijnissen, and B. Scarlett, *J. Aerosol Sci.* **30**, 823 (1999).

¹⁰A. J. Stone, *Science* **321**, 787 (2008).

¹¹*Glossary of Meteorology*, American Meteorological Society, 2nd ed. <http://amsglossary.allenpress.com/glossary> (Allen Press, Lawrence, Kansas, 2010).

¹²P. M. Tag, *J. Atmos. Sci.* **37**, 2347 (1980).